


Spin singlet and spin triplet pairing correlations on shape evolution in sd -shell $N = Z$ Nuclei

Eunja Ha* and Myung-Ki Cheoun†

Department of Physics and Origin of Matter and Evolution of Galaxy (OMEG) Institute, Soongsil University, Seoul 156-743, Korea

H. Sagawa‡

*RIKEN, Nishina Center for Accelerator-Based Science, Wako 351-0198, Japan
and Center for Mathematics and Physics, University of Aizu, Aizu-Wakamatsu, Fukushima 965-8560, Japan* (Received 7 November 2017; revised manuscript received 4 January 2018; published 16 February 2018)

We study the shape evolution of $N = Z$ nuclei ^{24}Mg , ^{28}Si , and ^{32}S in the axially symmetric deformed Woods-Saxon model, taking into account both $T = 0$ and $T = 1$ pairing interactions. We find the coexistence of $T = 0$ and $T = 1$ superfluidity phases in the large deformation region $|\beta_2| > 0.3$ in these three nuclei. The interplay between the two pairing interactions has an important effect on determining the deformation of the ground states in these nuclei. The self-energy contributions from the pairing correlations to the single particle (s.p.) energies are also examined.

DOI: [10.1103/PhysRevC.97.024320](https://doi.org/10.1103/PhysRevC.97.024320)

I. INTRODUCTION

Pairing correlations play important roles in nuclear structure and have an important effect on nuclear electromagnetic (EM) and weak transitions. The pairing correlations are classified into like-pairing [neutron-neutron (nn) and proton-proton (pp)] and unlike-pairing [neutron-proton (np)] correlations. In particular, for $N = Z$ nuclei, the np pairing may become significant because protons and neutrons occupy the same orbital and have the maximum configuration overlap, which makes especially $T = 0$ pairing important. The nn and pp pairings have an isovector (IV) spin-singlet ($T = 1, J = 0$) mode, while the np pairing correlations have peculiar isoscalar (IS) spin-triplet ($T = 0, J = 1$) as well as IV spin-singlet modes [1–5]. Over the last few decades, there have been many discussions regarding the np pairing correlations, in particular, the coexistence of IS and IV correlations and their competitions in some specific nuclear observables [6–12]. As shown in recent works [13,14], the nuclear structure of the $N \neq Z$ nuclei may also be affected by the np pairing correlations. For example, the authors of Ref. [13] found the mixing phase of the IS spin-triplet and IV spin-singlet condensation for nuclei with $60 < N < 70$ and $57 < Z < 64$.

Recently, interesting experimental data were reported, which showed more quenching in the IV $M1$ spin transition data than the IS ones for the $N = Z$ sd -shell nuclei [15]. These features are not expected from former theoretical discussions [16,17]. It was pointed out in Ref. [18] that the $T = 0$ pairing plays a significant role in causing these features in the spin-dependent observables.

The importance of the np pairing was also discussed in our early papers for double- β decay transitions calculated by a realistic two-body interaction given by the Brueckner G -matrix based on the CD Bonn potential [19,20]. These studies were performed using spherical QRPA, which did not include the deformation explicitly and the IS np pairing was taken into account by renormalizing the IV np pairing interactions.

The main aim of the present work is to study the shape evolution of sd -shell $N = Z$ nuclei in the deformed Bardeen-Cooper-Schrieffer (BCS) approach including all kinds of pairing correlations: IS and IV pairing correlations in the model. We will address also the self-energy term due to the pairing correlations in the BCS approach [21].

The deformation effect on $N = Z$ medium-heavy nuclei was discussed by deformed HF BCS model in Refs. [22,23] by Skyrme interactions and RMF model in Ref. [24]. However, the effect of $T = 0$ pairing correlations was not discussed in these works. This work is a general extension of the previous works [22,25–28].

This paper is presented as follows. In Sec. II, we briefly explain the deformed BCS method by a Woods-Saxon potential. In Sec. III, we discuss the shape evolution of the $N = Z$ sd -shell nuclei ^{24}Mg , ^{28}Si , and ^{32}S by a simple shell filling model and by the BCS theory. An evolution of the Fermi surface is also presented in terms of the deformation. Section IV is devoted to a summary and conclusions.

II. DEFORMED SINGLE-PARTICLE STATES

A deformed Woods-Saxon (WS) potential [29,30] is used to calculate Nilsson-type single-particle (s.p.) states. The single-particle spectrum obtained by the deformed WS potential (DWS) depends on the deformation parameters β_2 and β_4 . These parameters define explicitly the distance from the origin of the coordinate system to a point on the shape cut nuclear

*ejha@ssu.ac.kr

†Corresponding author: cheoun@ssu.ac.kr

‡sagawa@ribf.riken.jp

TABLE I. Deformation parameter β_2^{E2} from the experimental $E2$ transition data [34] and theoretical β_2 by relativistic mean field (RMF) [35] and FRDM model [36] for ^{24}Mg , ^{28}Si , and ^{32}S nuclei. $Q_{\text{exp.}}$ from experimental data [37,38] are also tabulated. Empirical pairing gaps are deduced from the five-point gap formulas in Eqs. (14) and (15) for Δ_p^{emp} and Δ_n^{emp} together with np pairing gap δ_{np}^{emp} obtained from Eq. (17).

Nucleus	β_2^{E2} [34]	β_2^{RMF} [35]	β_2^{FRDM} [36]	$Q_{\text{exp.}}$ [37,38]	Δ_p^{emp}	Δ_n^{emp}	δ_{np}^{emp}
^{24}Mg	0.605	0.416	0.	$-0.29 \sim -0.07$	3.123	3.193	1.844
^{28}Si (prolate)	0.407	x	x	x	2.841 ^a	2.917 ^a	1.384 ^a
^{28}Si (oblate)	x	-0.374	-0.363	0.16 \sim 0.18	2.841 ^a	2.917 ^a	1.384 ^a
^{32}S	0.312	0.186	0.221	$-0.12 \sim -0.18$	2.141	2.207	1.047

^aPairing gaps for ^{28}Si in Ref. [39] should be modified as these numbers.

surface

$$R(\theta, \beta_2, \beta_4) = R_0[1 + \beta_2 Y_{20}(\theta) + \beta_4 Y_{40}(\theta)], \quad (1)$$

where $R_0 = 1.2A^{1/3}\text{fm}$. Y_{20} and Y_{40} are the spherical harmonics. The customary parameter $\epsilon = 3(\omega_{\perp} - \omega_3)/(2\omega_{\perp} + \omega_3)$ used in the deformed harmonic oscillator is related to $\beta_2 \approx (2/3)\sqrt{4\pi/5}\epsilon$ at the leading order. In the cylindrical coordinate system, we define the axial symmetric deformed WS potential,

$$V_{\text{DWS}} = V_C + V_{SO} + V_{\text{Coul}}, \quad (2)$$

where the nuclear and spin-orbit potentials are given as [29,31]

$$V_C(l) = -\frac{V_0}{1 + \exp(l/a)}, \quad (3)$$

$$V_{SO}(l) = -\lambda(\hbar/2mc)^2[\nabla V(l)](\vec{\sigma} \times \vec{p}). \quad (4)$$

In Eqs. (3) and (4), l is a minimal distance function between a given point assigned by radial vector \vec{r} and the nuclear surface represented by Eq. (1). Here the minus sign is taken inside the surface. The Coulomb potential V_{Coul} is given in Ref. [29]. a and λ are diffuseness parameter and strength of a spin-orbit potential, respectively.

In general, the shell evolution by the deformation becomes significant in neutron-rich nuclei. The deformation can be confirmed by the $E2$ transition probability extracted from many experiments [32,33], and plays important roles in understanding the nucleosynthesis. Such features may also appear for deformed stable $N = Z$ nuclei. In particular, from the observed quadrupole moment Q_{2+} , ^{28}Si is known to be oblately deformed in contrast to other prolate deformations in ^{24}Mg and ^{32}S , according to recent data tabulated in Table I. However, in the β_2^{E2} from the $E2$ transition data in Table I, only absolute values are extracted and show no distinction between oblate and prolate shapes. These values (or experimental quadrupole moment Q_{2+}) are associated to an intrinsic deformation (or intrinsic quadrupole moment Q_0) in the rotational model, $Q_{J^{\pi}} = \frac{3K^2 - J(J+1)}{(J+1)(2J+3)} Q_0$. This relation is valid for well-developed intrinsic deformed nuclei, but is not always hold for lighter nuclei [40]. Since the nuclei considered in this work are not heavy, such a deformation index may not always come from the intrinsic deformation, but also expected to come from dynamical quadrupole vibration.

III. FORMALISM FOR DEFORMED BCS MODEL

We perform the deformed BCS calculations by using the deformed s.p. wave functions obtained from the potential in

Eq. (2). Since the theoretical framework for the deformed BCS approach had already been discussed in the previous paper [26], here only basic formulas are briefly stated. We perform also the deformed Hartree-Fock-Bogolyubov (HFB) calculations in the same context, but the results are almost equivalent to those of the deformed BCS ones. Because of this reason, we will not mention the results of deformed HFB in the present paper. We start from the following nuclear Hamiltonian:

$$\begin{aligned} H &= H_0 + H_{\text{int}}, \\ H_0 &= \sum_{\rho_{\alpha}\alpha\alpha'} \epsilon_{\rho_{\alpha}\alpha\alpha'} c_{\rho_{\alpha}\alpha\alpha'}^{\dagger} c_{\rho_{\alpha}\alpha\alpha'}, \\ H_{\text{int}} &= \sum_{\rho_{\alpha}\rho_{\beta}\rho_{\gamma}\rho_{\delta}, \alpha\beta\gamma\delta, \alpha'\beta'\gamma'\delta'} V_{\rho_{\alpha}\alpha\alpha'\rho_{\beta}\beta\beta'\rho_{\gamma}\gamma\gamma'\rho_{\delta}\delta\delta'} \\ &\quad \times c_{\rho_{\alpha}\alpha\alpha'}^{\dagger} c_{\rho_{\beta}\beta\beta'}^{\dagger} c_{\rho_{\delta}\delta\delta'} c_{\rho_{\gamma}\gamma\gamma'}, \end{aligned} \quad (5)$$

where Greek letters ($\alpha, \beta, \gamma, \delta$) denote real (bare) s.p. states with the absolute value of the angular momentum projection Ω of the angular momentum on a nuclear symmetry axis. The projection Ω is a good quantum number in the axial-symmetric deformed basis. ρ_{α} ($\rho_{\alpha} = \pm 1$) denotes a sign of the angular momentum projection Ω of the state assigned by the Nilsson quantum numbers α . Isospins of particles and quasiparticles are denoted by Greek letters with a prime ($\alpha', \beta', \gamma', \delta'$) and with a double prime ($\alpha'', \beta'', \gamma'', \delta''$), respectively. The operator $c_{\rho_{\alpha}\alpha\alpha'}^{\dagger}$ ($c_{\rho_{\alpha}\alpha\alpha'}$) in Eq. (5) stands for a creation (destruction) operator of the real particle in the state assigned by $\rho_{\alpha}\alpha'$ having the angular momentum projection Ω_{α} , its sign ρ_{α} , and the isospin α' . The Hamiltonian, represented by the real particles in Eq. (5), is then transformed to the quasiparticle representation through the deformed Bogolyubov transformation

$$\begin{aligned} a_{\rho_{\alpha}\alpha\alpha''}^{\dagger} &= \sum_{\rho_{\beta}\beta\beta'} (u_{\alpha\alpha''\beta\beta'} c_{\rho_{\beta}\beta\beta'}^{\dagger} + v_{\alpha\alpha''\beta\beta'} c_{\rho_{\beta}\beta\beta'}), \\ a_{\rho_{\alpha}\bar{\alpha}\alpha''} &= \sum_{\rho_{\beta}\beta\beta'} (u_{\bar{\alpha}\alpha''\beta\beta'} c_{\rho_{\beta}\beta\beta'} - v_{\bar{\alpha}\alpha''\beta\beta'} c_{\rho_{\beta}\beta\beta'}^{\dagger}). \end{aligned} \quad (6)$$

Our formalism is intended to include the np pairing correlations, so that we may denote the isospin of quasiparticles (α'' or β'') as = 1 or 2, while isospin of real particles (α' or β') is p or n . We assume the time reversal symmetry, which means $u_{\alpha\alpha''\beta\beta'} = u_{\beta\alpha''\bar{\alpha}\beta'}$ and $v_{\alpha\alpha''\beta\beta'} = -v_{\beta\alpha''\bar{\alpha}\beta'}$. In the deformed HFB (DHFB), the quasiparticle comprises particle and hole properties located in different deformed states, α and β . In the deformed BCS (DBCS), we do not allow the mixing of the different s.p. states,

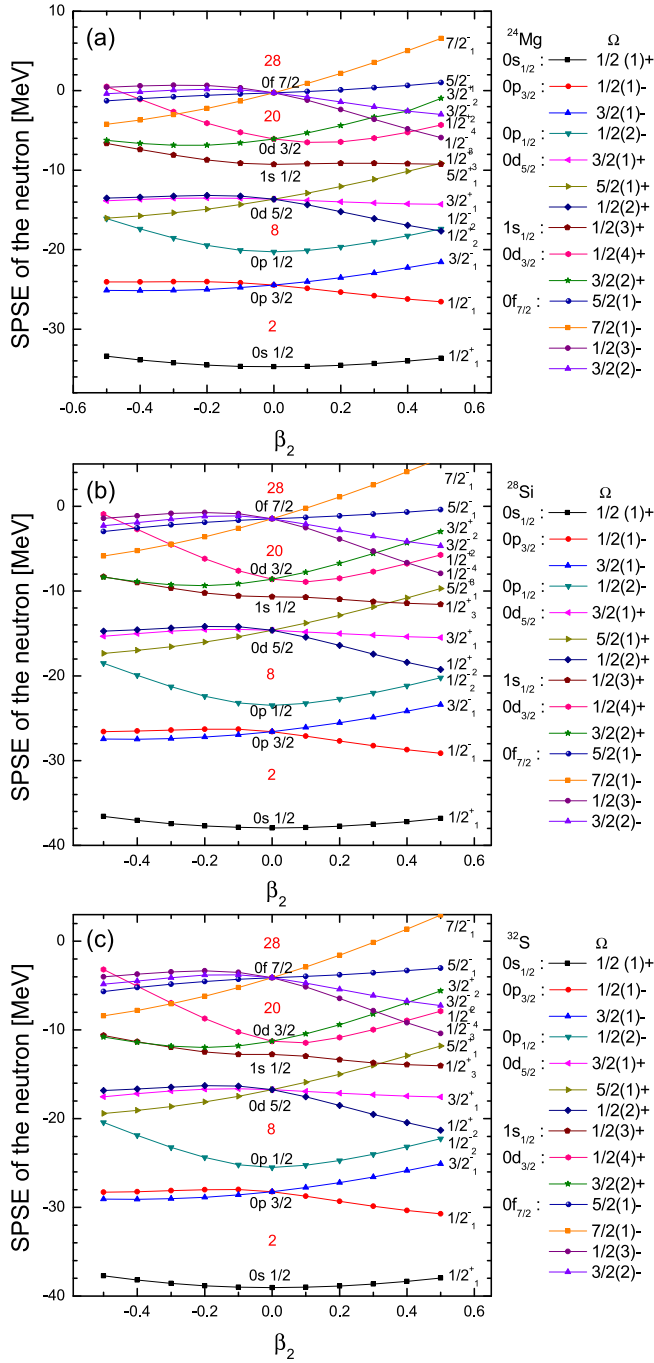


FIG. 1. (a–c) Shell evolutions of s.p. states by the deformation for ^{24}Mg , ^{28}Si , and ^{32}S . They are calculated by using a deformed Woods-Saxon potential with the optimal parameter set for ^{24}Mg and Chepurnov set for ^{28}Si and ^{32}S in Ref. [29].

α and β , to the quasiparticle in the deformed basis. However, in the view of the spherical basis, the quasiparticle state is a mixture of different particle states because each deformed state (basis) is represented by a linear combination of the spherical state (basis) (see Fig. 1 at Ref. [26]). This feature is one of additional characters coming from the inclusion of deformation in the BCS approach, i.e., the DBCS approach.

Consequently, the np pairing leads us to a HFB-type pairing potential constructed from many different states.

The DBCS transformation for each α state was then reduced to the following form:

$$\begin{pmatrix} a_1^\dagger \\ a_2^\dagger \\ a_{\bar{1}} \\ a_{\bar{2}} \end{pmatrix}_\alpha = \begin{pmatrix} u_{1p} & u_{1n} & v_{1p} & v_{1n} \\ u_{2p} & u_{2n} & v_{2p} & v_{2n} \\ -v_{1p} & -v_{1n} & u_{1p} & u_{1n} \\ -v_{2p} & -v_{2n} & u_{2p} & u_{2n} \end{pmatrix}_\alpha \begin{pmatrix} c_p^\dagger \\ c_n^\dagger \\ c_{\bar{p}} \\ c_{\bar{n}} \end{pmatrix}_\alpha. \quad (7)$$

The Hamiltonian can be expressed in terms of the quasiparticles as follows:

$$H' = H'_0 + \sum_{\rho_\alpha \alpha \alpha''} E_{\alpha \alpha''} a_{\rho_\alpha \alpha \alpha''}^\dagger a_{\rho_\alpha \alpha \alpha''} + H_{qp.int}. \quad (8)$$

Finally, using the transformation of Eq. (7), the following DBCS equation for each α state is obtained

$$\begin{pmatrix} \epsilon_p - \lambda_p & 0 & \Delta_{p\bar{p}} & \Delta_{p\bar{n}} \\ 0 & \epsilon_n - \lambda_n & \Delta_{n\bar{p}} & \Delta_{n\bar{n}} \\ \Delta_{p\bar{p}} & \Delta_{p\bar{n}} & -\epsilon_p + \lambda_p & 0 \\ \Delta_{n\bar{p}} & \Delta_{n\bar{n}} & 0 & -\epsilon_n + \lambda_n \end{pmatrix}_\alpha \begin{pmatrix} u_{\alpha''p} \\ u_{\alpha''n} \\ v_{\alpha''p} \\ v_{\alpha''n} \end{pmatrix}_\alpha = E_{\alpha \alpha''} \begin{pmatrix} u_{\alpha''p} \\ u_{\alpha''n} \\ v_{\alpha''p} \\ v_{\alpha''n} \end{pmatrix}_\alpha, \quad (9)$$

where $E_{\alpha \alpha''}$ is the energy of the quasiparticle with the isospin quantum number α'' in the state assigned by the label α . We include $n\bar{p}$ and $p\bar{n}$ pairings in addition to the usual $p\bar{p}$ and $n\bar{n}$ pairing correlations. The np and $\bar{n}\bar{p}$ pairings in the same orbital (e.g., $|np, T=0\rangle$ and $|\bar{n}\bar{p}, T=0\rangle$) are not included explicitly, but included implicitly by multiplying a factor of 2 on the $T=0$ matrices with $n\bar{p}$ and $p\bar{n}$ pairs. A detailed discussion of this procedure is done in Eqs. (22) and (23) in Sec. IV B. The pairing potentials for each α state in the DBCS are calculated in the deformed basis by using G matrices obtained from a realistic Bonn CD potential for nucleon-nucleon ($N-N$) interaction as follows:

$$\Delta_{p\bar{p}_\alpha} \equiv \Delta_{\alpha p\bar{p}} = - \sum_{J,c} g_{pp} F_{\alpha\bar{a}\bar{a}\alpha}^{J0} F_{\gamma c \bar{\gamma} c}^{J0} G(aacc, J, T=1) \times (u_{1p_c}^* v_{1p_c} + u_{2p_c}^* v_{2p_c}), \quad (10)$$

$$\Delta_{p\bar{n}_\alpha} \equiv \Delta_{\alpha p\bar{n}} = - \sum_{J,c} g_{np} F_{\alpha\bar{a}\bar{a}\alpha}^{J0} F_{\gamma c \bar{\gamma} c}^{J0} [G(aacc, J, T=1) \times \text{Re}(u_{1n_c}^* v_{1p_c} + u_{2n_c}^* v_{2p_c}) + iG(aacc, J, T=0) \times \text{Im}(u_{1n_c}^* v_{1p_c} + u_{2n_c}^* v_{2p_c})], \quad (11)$$

where Roman letters a and c stand for spherical s.p. state, i.e., $|a\Omega_\alpha\rangle = |N_0^a, l^a, \Lambda_\alpha^a, \Sigma^a\rangle$ and $|c\Omega_\alpha\rangle = |N_0^c, l^c, \Lambda_\alpha^c, \Sigma^c\rangle$. A coefficient $F_{\alpha\bar{a}\bar{a}\alpha}^{JK} = B_a^\alpha B_{\bar{a}}^\alpha (-1)^{J_a - \Omega_\alpha} C_{J_a \Omega_\alpha J_{\bar{a}} - \Omega_\alpha}^{JK}$ ($K = \Omega_\alpha - \Omega_{\bar{a}}$) is introduced to represent the G matrix in the deformed basis with an expansion coefficient B_a^α [28] from the spherical s.p.

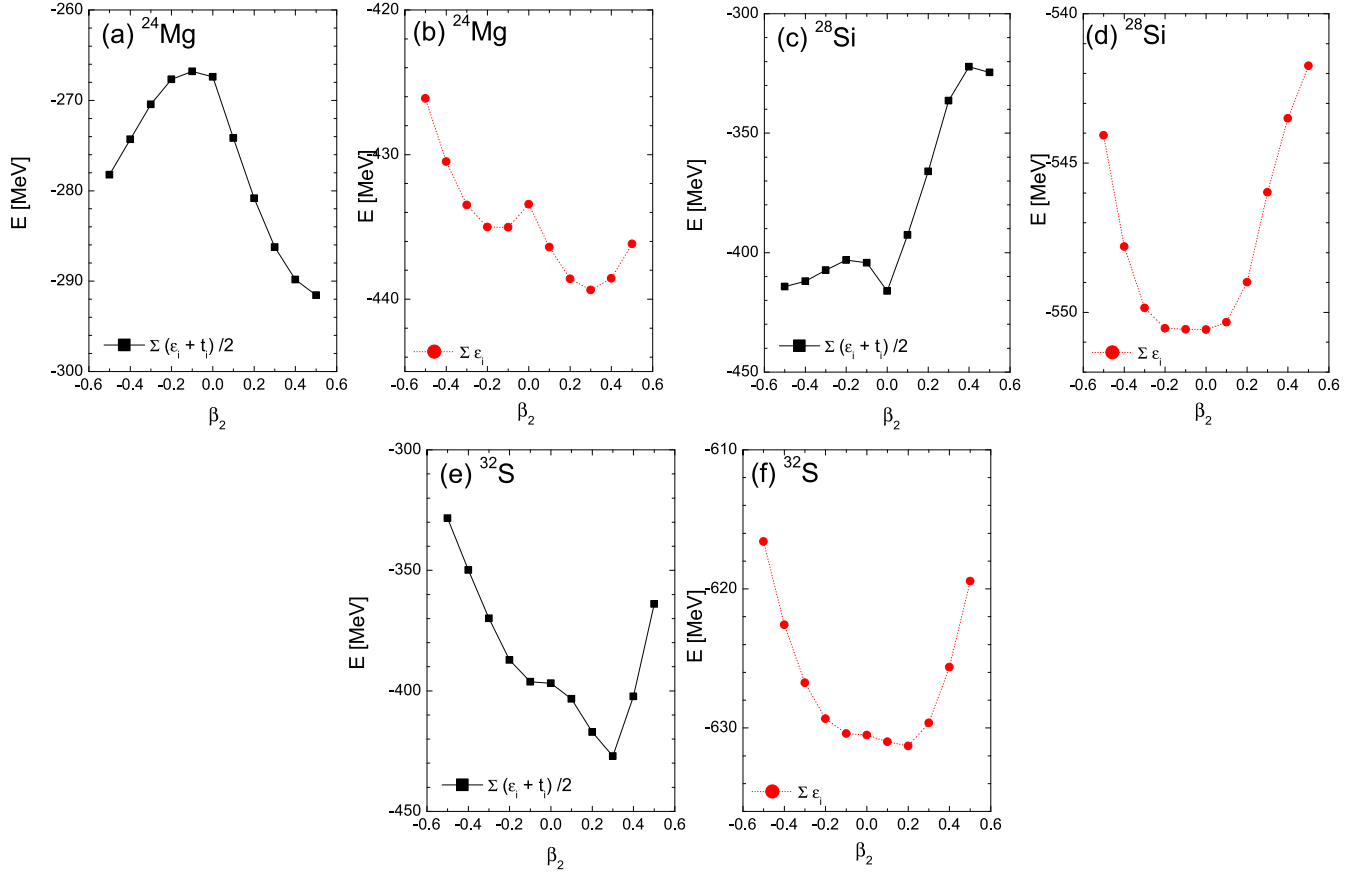


FIG. 2. (a,c,e) Ground-state energies (GSEs) and (b,d,f) total s.p. energies (TSPEs) by the filling approximation with the Woods-Saxon potential [29]. TSPEs are calculated by a sum of mean-field energies by Eq. (21), while GSEs are calculated by Eq. (20).

state to deformed s.p. state [26]

$$\begin{aligned}
 |\alpha\Omega_\alpha\rangle &\equiv \sum_{a\Sigma} B_a^\alpha |a\Omega_\alpha\rangle, \\
 B_a^\alpha &= \sum_{Nn_z\Sigma} C_{l\Lambda\frac{1}{2}\Sigma}^{j\Omega_\alpha} A_{Nn_z\Lambda}^{N_0l} b_{Nn_z\Sigma} \quad \text{with } A_{Nn_z\Lambda}^{N_0l n_r} \\
 &= \langle N_0l\Lambda | Nn_z\Lambda \rangle.
 \end{aligned} \tag{12}$$

In the coefficient $F_{\alpha\bar{a}\bar{a}\alpha}^{JK}$, K is a projection number of the total angular momentum J onto the z axis. It is selected to be $K = 0$ because we consider a pair of particles in the state α and its time-reversed state $\bar{\alpha}$. $G(acacJ)$ represents the two-body (pairwise) matrix element calculated in the spherical basis including all possible scattered pairs above Fermi surface. In the present work, we include all possible J values in Eqs. (10) and (11) by retaining the $K = 0$ projection. The neutron pairing gap $\Delta_{\alpha n \bar{\alpha} n}$ can be obtained by replacing n by p in Eq. (10).

In this work, the self-energy term due to the pairing correlations is introduced in the $\epsilon_{p(n)} - \lambda_{p(n)}$ for each α state in Eq. (9)

$$\mu_\alpha^{p(n)} = \frac{-1}{2} \sum_{J,c} F_{\alpha\bar{\alpha}\bar{\gamma}c}^{J0} F_{\alpha\bar{\alpha}\bar{\gamma}c}^{J0} G(acac, J) (v_{1p(n)c}^2 + v_{2p(n)c}^2), \tag{13}$$

which is usually neglected in the BCS equation because it comes from particle-hole correlations beyond the BCS. To see quantitatively its effect on the deformed s.p. state, we include the self-energy contributions, Eq. (13),

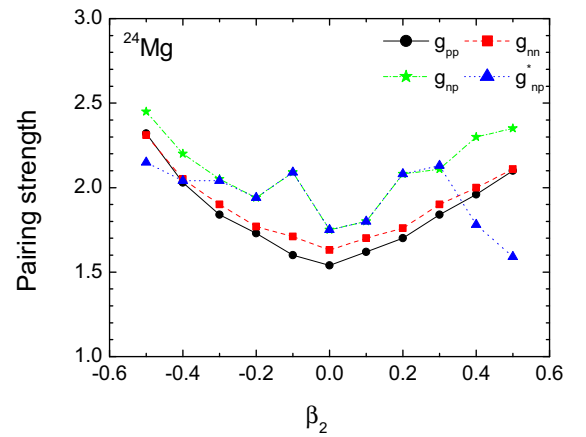


FIG. 3. Evolution of np pairing strength for ^{24}Mg in term of the deformation. The g_{nn}, g_{pp} , and g_{np} in Eqs. (10) and (11) are adjusted to reproduce empirical pairing gaps in Table I. The values g_{np}^* are adjusted by using the enhanced $T = 0$ interaction of the np channel. See the text for details.

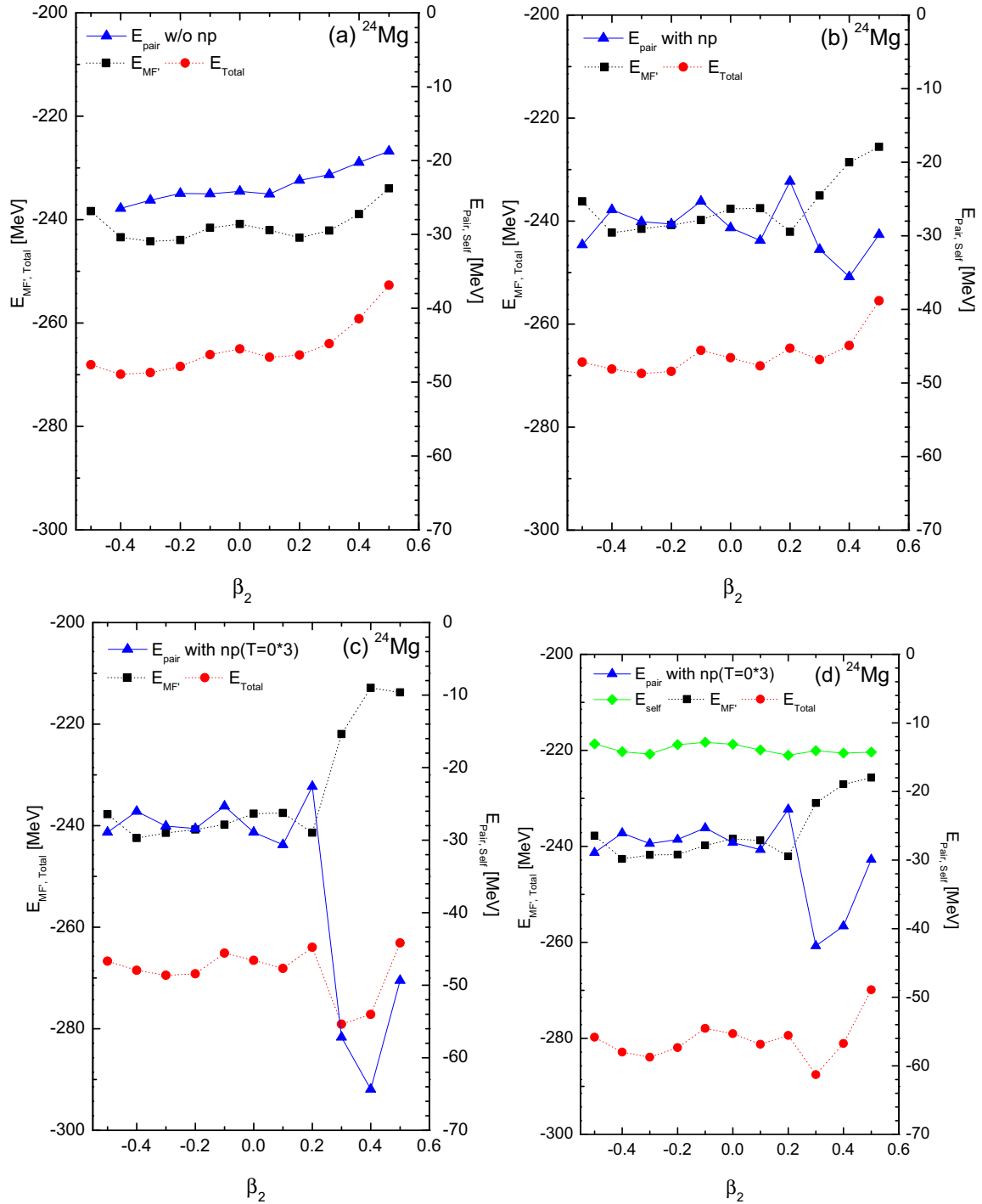


FIG. 4. The ground-state energy ($E_{GSE'} = E_{MF'} + E_{pair} + E_{self}$), which is termed as E_{total} denoted as red points, by the DBCS model for ^{24}Mg with a deformed Woods-Saxon potential [29] with respect to the DBCS Fermi energy. Mean-field energy by the DBCS is denoted as $E_{MF'}$. Notice that $E_{MF'}$ is different from the E_{GSE} obtained by the filling model in Fig. 2 because the Fermi energy is changed by the BCS approach owing to the pairing interactions. E_{pair} is the pairing energy referred to by the right y axis. The pairing energies are estimated by three different cases, without and with the np pairing in panels (a) and (b), respectively, and with the enhanced $T = 0$ pairing in np channel in panel (c). The last one (d) is results including the self-energy in Eq. (13).

to Eq. (9). As shown later, the self-energy turns out to give sizable contributions to total energies of relevant nuclei.

For the gap equations, Eqs. (10) and (11), we introduce renormalized parameters g_{pp} and g_{nn} , which are multiplied to the G matrix [19], so that the calculated pairing gaps $\Delta_{p\bar{p}}$ and

$\Delta_{n\bar{n}}$ in Eq.(10) reproduce the empirical pairing gaps Δ_p^{emp} and Δ_n^{emp} . The empirical pairing gaps of protons and neutrons are evaluated by the five-point formulas for neighboring nuclei [41]

$$\Delta_p^{\text{emp}} = \frac{1}{8}[M(Z+2, N) - 4M(Z+1, N) + 6M(Z, N) - 4M(Z-1, N) + M(Z-2, N)], \quad (14)$$

$$\Delta_n^{\text{emp}} = \frac{1}{8}[M(Z, N+2) - 4M(Z, N+1) + 6M(Z, N) - 4M(Z, N-1) + M(Z, N-2)]. \quad (15)$$

For np pairing correlations, we assume that the ground state of odd-odd nuclei has one proton and one neutron outside of even-even core embedding close to the Fermi surface. Furthermore, two particles are influenced under the attractive np pairing interaction [4,19]. Therefore masses of the odd-odd nuclei are treated as a sum of even-even mass and the proton and the neutron pairing gaps subtracted by the attractive residual np interaction energy

$$M(Z, N)_{\text{odd-odd}} = M(Z, N)_{\text{even-even}} + \Delta_p^{\text{emp}} + \Delta_n^{\text{emp}} - \delta_{np}^{\text{emp}}. \quad (16)$$

Then the np pairing gap is deduced as follows:

$$\begin{aligned} \delta_{np}^{\text{emp}} = & \pm \frac{1}{4}\{2[M(Z, N+1) \\ & + M(Z, N-1) + M(Z-1, N) + M(Z+1, N)] \\ & - [M(Z+1, N+1) + M(Z-1, N+1) \\ & + M(Z-1, N-1) + M(Z+1, N-1)] \\ & - 4M(Z, N)\}, \end{aligned} \quad (17)$$

where the signs in the $+(-)$ stand for even (odd) mass nuclei. In the present model, theoretical np pairing gaps are calculated as

$$\delta_{np}^{\text{th}} = -[(H_{gs}^{12} + E_1 + E_2) - (H_{gs}^{np} + E_p + E_n)]. \quad (18)$$

Here $H_{gs}^{12}(H_{gs}^{np})$ is the total deformed BCS ground-state energy with (without) np pairing and $E_1 + E_2(E_p + E_n)$ is a sum of the lowest two quasiparticle energies with (without) the np pairing potential Δ_{np} in Eq. (9). All of the pairing gaps exploited in this work are tabulated in Table I. Our theoretical pairing gaps are fitted within a few percent ambiguity to the empirical values by adjusting the pairing strengths g_{nn}, g_{pp}, g_{np} , in Eqs. (10) and (11).

For a more quantitative argument on the np pairing gaps, one should eliminate spurious components in the wave functions due to fluctuations of the particle number and isospin quantum number in the BCS approach. More refined approaches might be desired, such as the (isospin) generalized BCS [3,6], which includes $|np\rangle$ and $|\bar{n}\bar{p}\rangle$ pairing as well as $|n\bar{p}\rangle$ and $|p\bar{n}\rangle$ pairing considered in this work, and the projected BCS for the exact particle and isospin quantum number conservations. These studies remain for future projects.

IV. RESULTS AND DISCUSSIONS

This study adopts the optimal and Chepurinov parameter sets for the axially symmetric Woods-Saxon potential given

by Cwiok *et al* [29]. Other parameter sets show almost the same results for the nuclei considered in this work [39]. The model space for all the nuclei was taken up to $N = 5\hbar\omega$ for the deformed basis and up to $N = 10\hbar\omega$ for the spherical basis. Results of the evolution of s.p. states by the deformation parameter β_2 are shown in Fig. 1. First we consider a simple shell-filling model, in which all particles distribute from the bottom of the potential up to the outermost shell orbit by allocating two particles in each s.p.state. The shell structure of ^{24}Mg and ^{32}S [Figs. 1(a) and 1(c)] are evolved from an open shell to a closed shell nature along the change of spherical to prolate deformation. However, for ^{28}Si [Fig. 1(b)], the evolution is different from the two nuclei, i.e., it evolves from a closed shell to an open shell nature as β_2 increases.

The increase of s.p.states energy of $5/2^+$ state ($N = 2, n_z = 0, \Lambda = 2, \Omega = 5/2$ in Nilsson quantum number) is a key ingredient for the shell evolution of the nuclei and can be easily understood by the asymptotic formula of anharmonic oscillator (AHO) energy;

$$\epsilon_{\text{AHO}}(n_z, n_\rho, m_l) \sim \hbar\omega_0[(N + 3/2) + \beta_2(N/3 - n_z)], \quad (19)$$

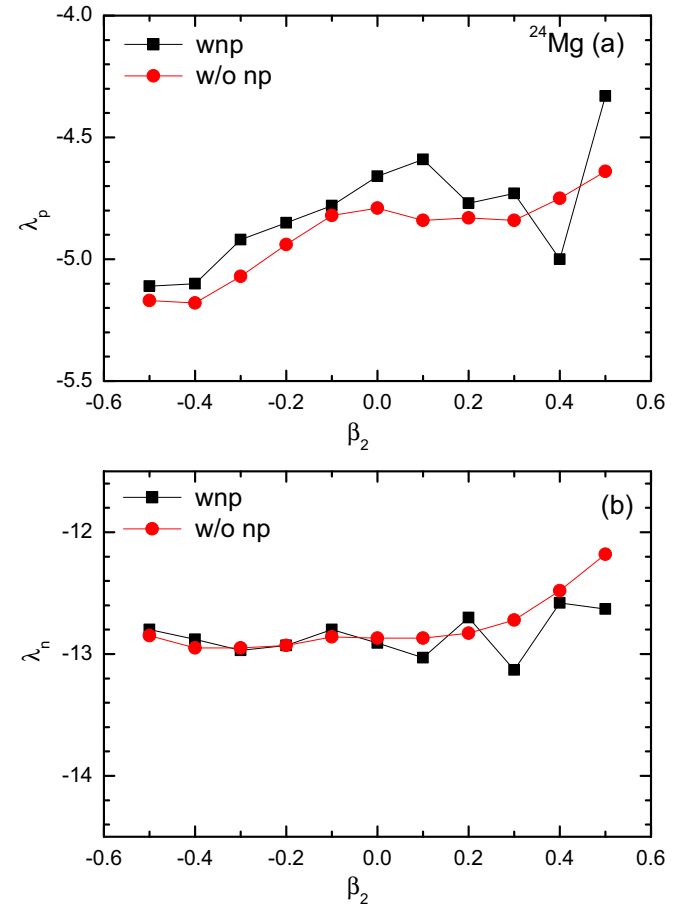
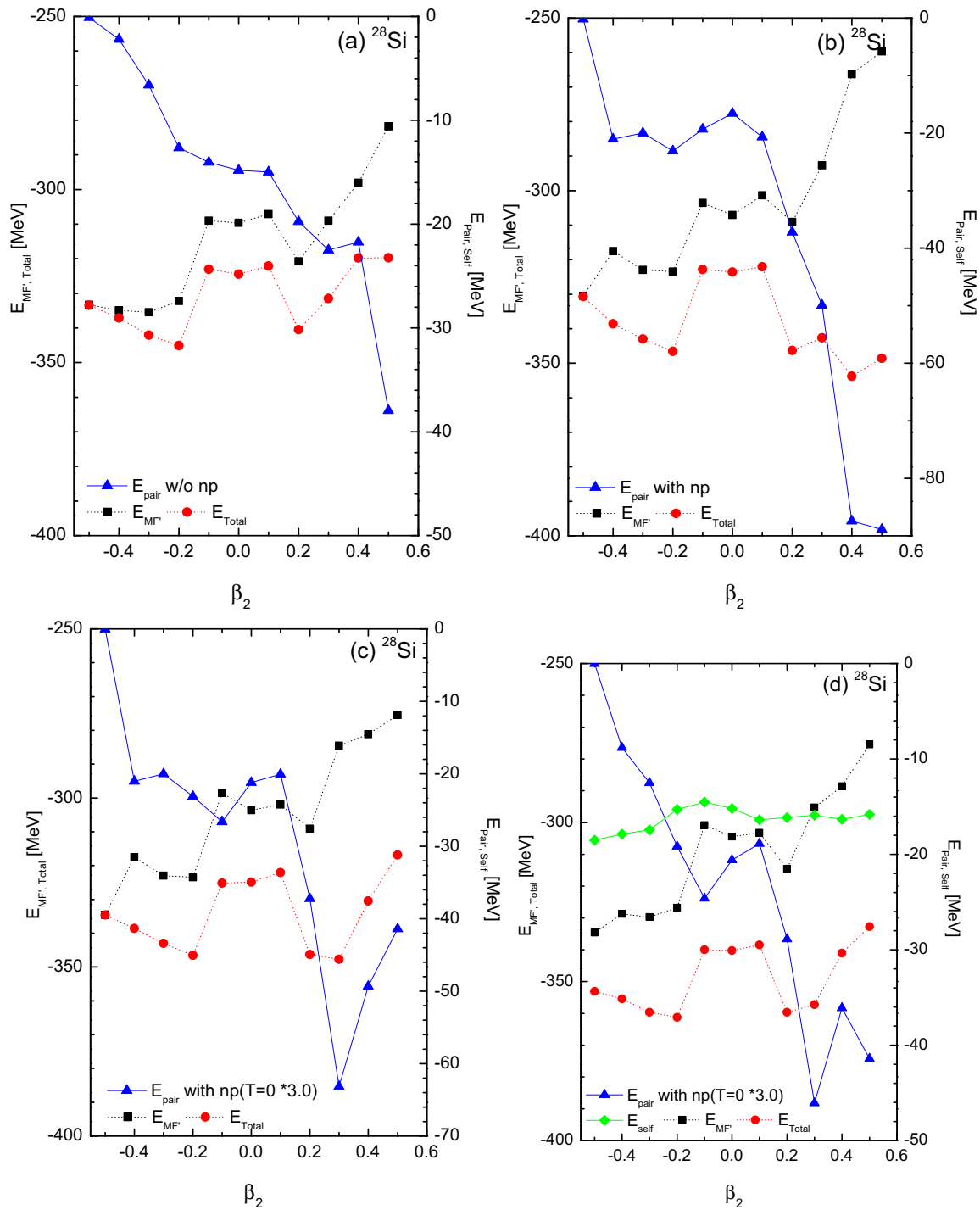


FIG. 5. Evolution of the proton and neutron Fermi energies (the chemical potentials λ_p and λ_n) for ^{24}Mg as a function of the deformation β_2 with and without the np pairing correlations.


 FIG. 6. The same as Fig. 4, but for ^{28}Si .

where the last term stands for the deformation effect. Since the orbit $5/2_1^+$ has $N = 2$ and $n_z = 0$, it goes up to higher energy with the positive (prolate) deformation. In Figs. 1(b) and 1(c), the crossing between the $5/2_1^+$ state and $1/2_3^+$ ($[N, n_z, 2, \Lambda, \Omega] = 2, 1, 1, 1/2$) state happens around the $\beta_2 = 0.3\text{--}0.4$ region. This crossing also affects the evolution of the Fermi energies identified as the outermost occupied state.

A. Results by the filling approximation model

In Fig. 2, we show evolutions of the ground-state energy (GSE) defined by

$$E_{\text{GSE}} = \sum_i^{A/2} \frac{1}{2} [(\epsilon_i^p + t_i^p) + (\epsilon_i^n + t_i^n)] \quad (20)$$

with kinetic energy t_i [42]. The ground-state energy E_{GSE} is calculated referring to the highest occupied orbit (HOO) as the Fermi energy and taken to be zero energy, i.e., $\epsilon_i(\text{HOO}) = 0$. We also show a sum of s.p. energies of all occupied orbits,

$$E_{\text{TSPE}} = \sum_{i=1}^{Z/2(N/2)} (\epsilon_i^p + \epsilon_i^n) \quad (21)$$

as a reference to see the relation between the shell evolution and the Nilsson s.p. energy. The energies in Eqs. (20) and (21) are calculated by the filling approximation in which the occupation probabilities are taken as $v_i^2 = 1$ for the orbit from the bottom of the potential to the HOO state. Otherwise $v_i^2 = 0$ for the unoccupied orbits. Two results show a different evolution as a function of the β_2 deformation, in particular, in the oblate deformation region of ^{24}Mg and ^{28}Si . The reason turns out to come from the different energy evolution of the HOO state as will be discussed in the following.

Different evolutions of the TSPEs by the prolate and oblate deformation can be easily understood by the evolution of the HOO energy in Fig. 1. The uphill shapes by the prolate deformation in Figs. 2(c) to 2(f) for ^{28}Si and ^{32}S come from the energy increase of the HOO $5/2_1^+$ state, which makes the binding of HOO state more loosely at the prolate deformation. The downhill shape in TSPEs in Fig. 2(b) for ^{24}Mg is mainly due to the decrease of s.p. energy of the outermost HOO $1/2_2^+$ state for larger deformations. However, the shell evolution in the GSE by DWS calculations reveals a different shape evolution, especially in Figs. 2(a) and 2(c) for ^{24}Mg and ^{28}Si because the HOO energy may also be changed as a function of deformation. The present situation will be largely changed by the pairing correlations, which makes a wide smearing of the occupation probabilities of states near the Fermi level as will be discussed in the next subsection.

B. Results by the deformed BCS calculations with $T = 0$ and $T = 1$ pairing correlations

Here we calculate the GSE evolution by the DBCS model, which takes into account the np pairing as well as the nn and pp pairing correlations. We study the pairing correlations for four different cases in Figs. 4, 6, and 8. The first two cases are (a) without and (b) with the np pairing correlations. The 3rd one (c) is with the enhanced $T = 0$ pairing of np channel, and the last one (d) is done by taking the self-energy term Eq. (13) into the case (c). The ground-state energy, E_{GSE} , termed as E_{Total} denoted by red points in the figure, by the DBCS model comprises the mean field energy, E_{MF} , the pairing energy E_{pair} . The self energy is included in panel (d). Here the mean-field energy, E_{MF} , is calculated similarly to the GSE results by Eq. (20) in Fig. 2 with respect to the Fermi energies $\lambda_{n,p}$ taken as zero energy.

Usually the $T = 0$ channel in the np pairing was not strong enough to manifest itself in the pairing energy [4,26]. However, recent experimental $M1$ spin transition data for the $N = Z$ sd -shell nuclei [15] show that a summed isovector spin strength is much more quenched than a sum of isoscalar spin strengths in the same energy region. This evidence is considered as a sign of strong $T = 0$ pairing correlations in the ground states of $N =$

Z nuclei [43]. The signature of strong $T = 0$ pairing was also found in the GT transitions in $N = Z$ and $N = Z + 2$ nuclei [14,18]. Therefore, in the third case, we adopt a strong isoscalar pairing effect by multiplying a factor 1.5 to the corresponding $T = 0$ matrices obtained from the G -matrix calculations.

In the present scheme, we include only $n\bar{p}$ and $\bar{p}n$ pairing correlations, but do not explicitly include the np and $\bar{n}\bar{p}$ pairings. We effectively include these $T = 0$ contributions of the np and $\bar{n}\bar{p}$ channels by multiplying another factor 2 to the $T = 0$ pairing matrices of the $n\bar{p}$ and $p\bar{n}$ configurations. This procedure can be justified as follows. By following Ref. [3], for np , $\bar{n}\bar{p}$, $\bar{n}p$ and $n\bar{p}$ pairings, if we assume

$$\begin{aligned} \langle \alpha n \alpha p, T = 0 | V_{\text{pair}} | \beta n \beta p, T = 0 \rangle = \\ \langle \alpha n \alpha p, T = 0 | V_{\text{pair}} | \bar{\beta} n \bar{\beta} p, T = 0 \rangle, \end{aligned} \quad (22)$$

then $\text{Im} \Delta_{\alpha n \alpha p}^{T=0} = 0$ and $\text{Re} \Delta_{\alpha n \alpha p}^{T=0} = \text{Im} \Delta_{\alpha n \bar{\alpha} p}^{T=0}$ by Eqs. (5) to (7) in Ref. [3]. It leads to

$$\Delta_{np}^{2(T=0)} = 2|\Delta_{\alpha p \bar{\alpha} n}^{T=0}|^2 + 2|\Delta_{\alpha p \alpha n}^{T=0}|^2 = 4|\Delta_{\alpha p \bar{\alpha} n}^{T=0}|^2, \quad (23)$$

where a factor of 2 in the second term is due to $\bar{\alpha} p \alpha n$ and $\bar{\alpha} p \bar{\alpha} n$ pairings, respectively. Consequently, we multiply a weighting factor of $1.5 \times 2 = 3.0$ on the $T = 0$ pairing G -matrix strength for the cases (c) and (d) in Figs. 4, 6, and 8.

In Fig. 3, the pairing coupling strengths g_{nn}, g_{pp} and g_{np} in Eqs. (10) and (11) are plotted as a function of deformation parameter β_2 for ^{24}Mg . They are obtained in such a way that calculated gaps reproduce the empirical ones in Table I. In general, we need a larger coupling strength for larger prolate and oblate deformations to reproduce the empirical pairing gaps because of the closed-shell nature at larger deformations. One may find interestingly different behavior of curves of g_{np} and g_{np}^* for larger deformation $|\beta_2| > 0.3$. One can notice that g_{np} and g_{np}^* are almost the same value in the region $|\beta_2| \leq 0.3$. That is, the $T = 0$ pairing correlations do not contribute to the pairing gaps at all. However g_{np}^* becomes smaller in both larger prolate and oblate deformation region $|\beta_2| \geq 0.3$. This is due to the effect of the $T = 0$ pairing condensation which makes an additional $T = 0$ correlations to the gap energy usually dominated by the $T = 1$ np contributions. These results suggest a manifestation of the coexistence of

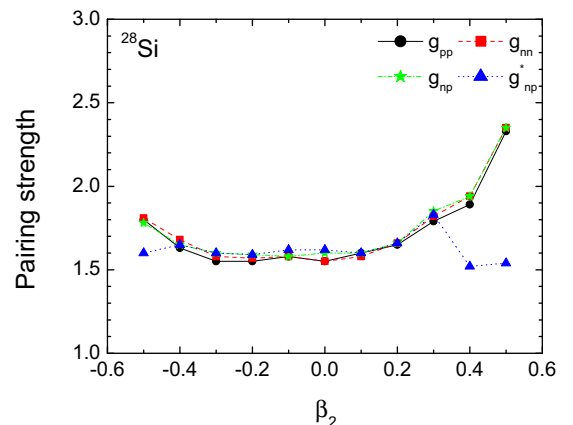
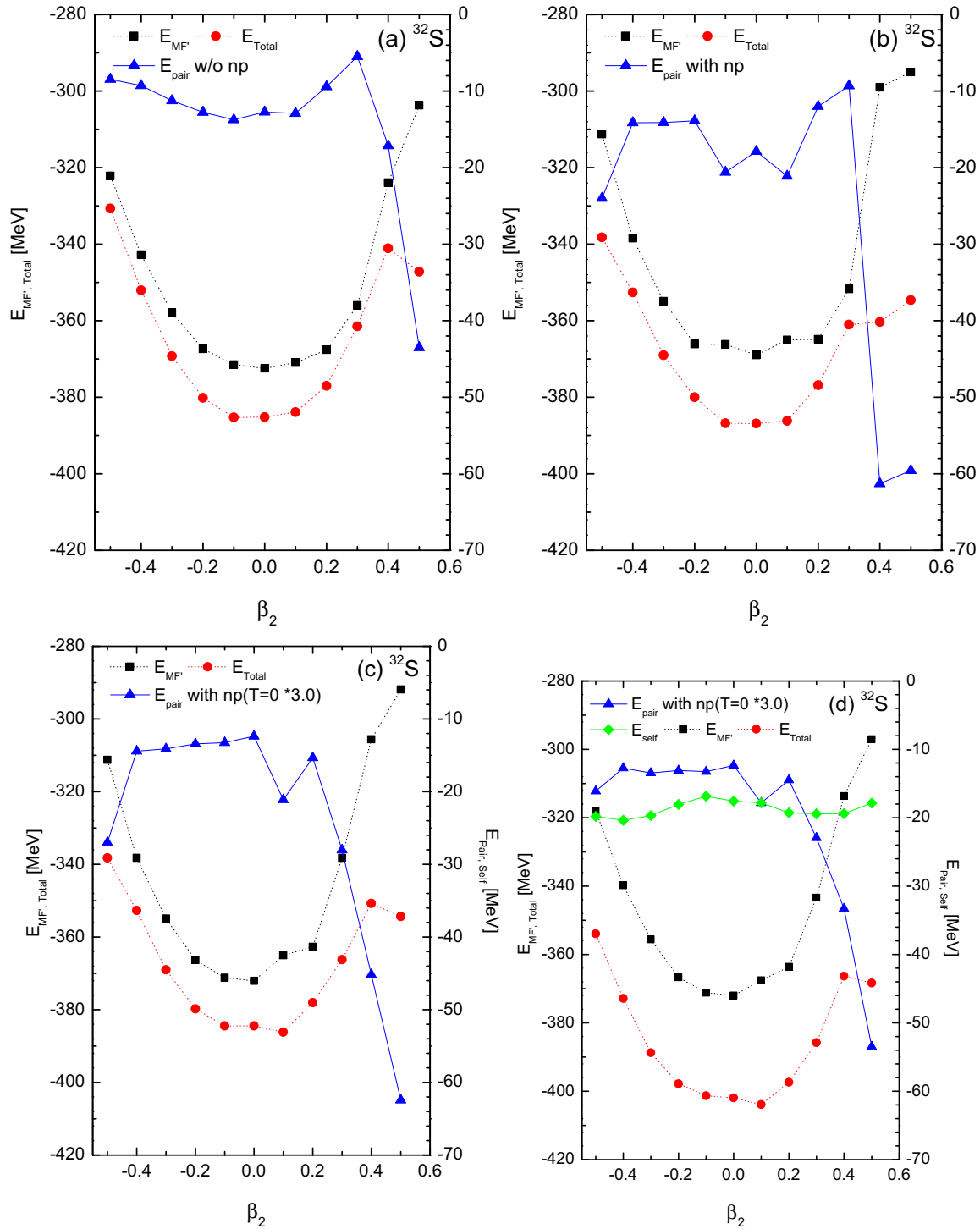


FIG. 7. Same as Fig. 3, but for ^{28}Si .


 FIG. 8. The same as Fig. 4, but for ^{32}S .

two types of superconductivities ($T = 0$ and $T = 1$) in this large deformed region.

In the following we present numerical DBCS results of the ground state energies (GSEs) for ^{24}Mg , ^{28}Si , and ^{32}S in terms of the deformation parameter β_2 . We examine also the effect of the self-energy in the DBCS approach in Fig. 4(d).

I. ^{24}Mg

Mean-field energy for ^{24}Mg , E_{MF} , by the DBCS is calculated by the formula, $\Sigma_i(\epsilon_i + t_i)v_i^2/2$, with respect to the Fermi energy ϵ_f . The energy ($E_{\text{GSE}} = E_{\text{total}} = E_{\text{MF}} + E_{\text{pair}} + E_{\text{self}}$) corresponds to the total ground-state energy E_{GSE} in DWS calculations with filling approximation. The results in Fig. 4(a) show two shallow minima in both prolate and oblate regions.

The pairing energy E_{pair} , without the np in Fig. 4(a) turns out to be smaller for the prolate deformation, but becomes somewhat larger by the np pairing correlations. This is simply due to a larger level density in the oblate side than that of prolate side which can be seen in Fig. 1(a).

The evolution of Fermi energy ϵ_f (equivalently the chemical potentials λ) is shown in Fig. 5 which is a key factor to understand the evolution of the total energy. Without np pairing, one can find an increase of the Fermi energy for larger prolate deformation, which originates from the evolution of s.p. energy of $5/2_1^+$ state in Fig. 1(a). The np pairing changes the Fermi energy gap, by which the pairing energy becomes stronger as shown in Figs. 4(b) and 4(c). However, the pairing energy contribution to total energy is small compared to the mean-field energy E_{MF} (Note the different energy scale in right for the pairing and left y axis for the total energy), so that the total energy minimum locates still in the oblate region in Fig. 4(b).

In the Fig. 4(c) we use the enhanced $T = 0$ interaction, which makes the pairing correlations stronger especially at the large prolate deformation and leads to the prolate deformation minimum in ^{24}Mg . A drastic change of the pairing correlation energy is induced by the active $T = 0$ pairing channel as was shown also in Fig. 3. Figure 4(d) shows results with the self-energy terms. The self-energy does not much affect the shape evolution of ^{24}Mg because the self-energy contributions denoted by green diamonds are approximately constant, to be 15 MeV with about 2–3 MeV variations.

2. ^{28}Si

The energy evolution of ^{28}Si is displayed in Fig. 6. Without the np pairing shown in Fig. 6(a), we can see two deformation minima at both the oblate and prolate sides at around $\beta_2 = \pm 0.2$. The pairing correlations are larger at larger prolate deformation to be $E_{\text{pair}} \sim 40$ MeV at $\beta_2 = 0.5$ and almost disappear at larger oblate deformation. These features are entirely determined by the nature of level density around the Fermi energy, i.e., very high level density at larger prolate deformation and very low at larger oblate side, In Fig. 6(b) with np pairing correlations, the pairing gain energy is much larger than the case without np pairing in Fig. 6(a). Here E_{pair} in Figs. 6(c) and 6(d) with the enhanced $T = 0$ pairing is smaller than Fig. 6(b) in the $\beta_2 > 0.3$ prolate region. It comes from the fact in Fig. 7, where the g_{np} and g_{np}^* show almost the same strength up to $\beta_2 = 0.3$, but the g_{np}^* becomes smaller than g_{np} in the region $\beta_2 > 0.3$. Because of the $T = 0$ superfluidity, the isoscalar coupling does not need to be larger to reproduce the empirical pairing gap δ_{np}^{emp} . While the gap index δ_{np} is the same for Figs. 6(b) and 6(c), the correlation energy in Fig. 6(b) is larger than that of Fig. 6(c). One more point is that contributions of E_{MF} and E_{pair} are not the same in Figs. 6(c) and 6(d) although the value g_{np}^* is the same. It stems from the self-energy term which will change the occupation probabilities through the normalized s.p. energies, and also E_{MF} and E_{pair} . But the self-energy contribution E_{self} in Fig. 6(d) is rather independent to the change of deformation to be about $E_{\text{self}} \sim 16$ MeV.

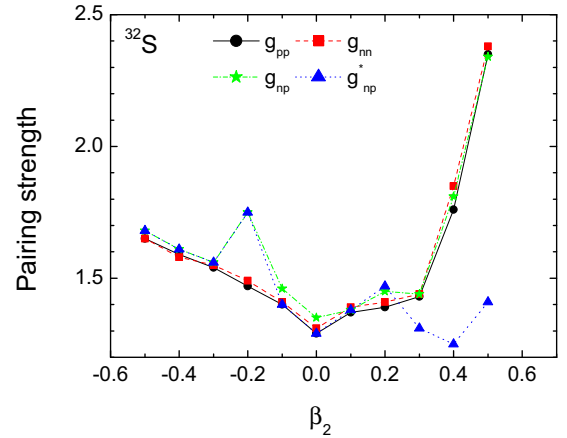


FIG. 9. Same as Fig. 3, but for ^{32}S .

3. ^{32}S

Calculated results of ^{32}S with $T = 1$ pairing without np pairing show a shallow energy minimum at $\beta_2 \sim 0.0$ in Fig. 8(a). The pairing gain energy is relatively small as $E_{\text{gain}} \sim 10$ MeV compared to the other two nuclei except at very large deformation $\beta_2 \sim 0.5$. This is again entirely due to the low level density around the Fermi energy of ^{32}S with $N = Z = 16$ except at the large deformation region where the level density becomes high. We can see in Fig. 8(b) larger pairing correlation energies with np pairing. The enhanced $T = 0$ pairing interaction in Figs. 8(c) and 8(d) gives a rather shallow energy minimum at a small prolate deformation $\beta_2 \sim 0.1$. The self-energy terms E_{self} give again constant contributions to the total energies and do not change the position of deformation minimum appreciably. Here we also find the similar behavior of pairing energy to that of ^{28}Si due to the change of the enhanced $T = 0$ pairing strength in Fig. 9 in the prolate deformed $\beta_2 > 0.3$ region.

In Ref. [11], the effect of deformation on the coexistence between neutron-proton and like-particle (proton-proton and neutron-neutron) pairings were studied in fp -shell even-even self-conjugate nuclei by using a model combining self-consistent mean-field and shell-model techniques. In their approach, the self-consistent mean-field calculations provide the main ingredients, single-particle energies, and residual two-body matrix elements, that are used in the subsequent shell model calculations to obtain the pairing correlation energies. It was found that the IS np pairing is generally much weaker than the IV contribution. However, in some cases, it was pointed out that large deformation induces the coexistence of IS and IV np pair condensates. While the model and masses of nuclei studied in Ref. [11] are different from the present ones, the two models draw the same conclusion about the importance of deformation on the coexistence of two superfluidity.

V. SUMMARY AND CONCLUSION

We study the shape evolution of $N = Z$ nuclei, ^{24}Mg , ^{28}Si , and ^{32}S in the DWS and DBCS approximations taking into account both $T = 0$ and $T = 1$ pairing correlations. In the

filling approximation for the DWS potential, it is shown that the shape evolution correlates strongly with the shell structure of s.p. energies near the last occupied orbit (Fermi energy). The effect of two types of pairing correlations with the isospin $T = 0$ and $T = 1$ are studied by the DBCS model with G -matrix-based pairing interactions. We adopt an enhanced $T = 0$ pairing interaction to clarify the effect of $T = 0$ pairing on the ground-state energy. We find a coexistent phase of two types of superconductors in the large deformation region $|\beta_2| > 0.3$ in ^{24}Mg , ^{28}Si , and ^{32}S with the enhanced $T = 0$ pairing. The competition between $T = 0$ and $T = 1$ pairing channels gives a substantial effect on the energy minima of ^{24}Mg , ^{28}Si , and ^{32}S . Our model gives reasonable deformation minima for these

nuclei, prolate for ^{24}Mg and ^{32}S , and oblate for ^{28}Si . The self-energy terms turn out to be rather constant as a function of deformation in the three nuclei and do not change appreciably the shape evolution.

ACKNOWLEDGMENTS

This work was supported by the National Research Foundation of Korea (Grants No. NRF-2015R1D1A4A01020477, No. NRF-2017R1E1A1A01074023, and No. NRF-2015K2A9A1A06046598). This work was also supported, in part, by JSPS KAKENHI Grant No. JP16K05367.

-
- [1] H. T. Chen and A. Goswami, *Phys. Lett. B* **24**, 257 (1967).
 [2] H. H. Wolter, A. Faessler, and P. U. Sauer, *Phys. Lett. B* **31**, 516 (1970).
 [3] A. L. Goodman, *Phys. Rev. C* **58**, R3051 (1998).
 [4] F. Šimkovic, C. C. Moustakidis, L. Pacearescu, and A. Faessler, *Phys. Rev. C* **68**, 054319 (2003).
 [5] S. Frauendorf and A. O. Miacchiavelli, *Prog. Part. and Nucl. Phys.* **78**, 24 (2014).
 [6] J. Engel, S. Pittel, M. Stoitsov, P. Vogel, and J. Dukelsky, *Phys. Rev. C* **55**, 1781 (1997).
 [7] O. Civitarese, M. Reboiro, and P. Vogel, *Phys. Rev. C* **56**, 1840 (1997).
 [8] J. Engel, K. Langanke, and P. Vogel, *Phys. Lett. B* **389**, 211 (1996).
 [9] W. Satula and R. Wyss, *Phys. Lett. B* **393**, 1 (1997).
 [10] K. Yoshida, *Phys. Rev. C* **90**, 031303(R) (2014).
 [11] D. Gambacurta and D. Lacroix, *Phys. Rev. C* **91**, 014308 (2015).
 [12] B. Bulthuis and A. Gezerlis, *Phys. Rev. C* **93**, 014312 (2016).
 [13] A. Gezerlis, G. F. Bertsch, and Y. L. Luo, *Phys. Rev. Lett.* **106**, 252502 (2011).
 [14] C. L. Bai, H. Sagawa, M. Sasano, T. Uesaka, K. Hagino, H. Q. Zhang, X. Z. Zhang, and F. R. Xu, *Phys. Lett. B* **719**, 116 (2013).
 [15] H. Matsubara *et al.*, *Phys. Rev. Lett.* **115**, 102501 (2015).
 [16] A. Arima, K. Shimizu, W. Bentz, and H. Hyuga, *Adv. Nucl. Phys.* **18**, 1 (1987).
 [17] I. S. Towner, *Phys. Rep.* **155**, 263 (1987).
 [18] H. Sagawa, C. L. Bai, and G. Colo, *Phys. Scr.* **91**, 083011 (2016).
 [19] M. K. Cheoun, A. Bobyk, A. Faessler, F. Šimkovic, and G. Teneva, *Nucl. Phys. A* **561**, 74 (1993); **564**, 329 (1993); M. K. Cheoun, A. Faessler, F. Šimkovic, G. Teneva, and A. Bobyk, *ibid.* **587**, 301 (1995).
 [20] G. Pantis, F. Šimkovic, J. D. Vergados, and A. Faessler, *Phys. Rev. C* **53**, 695 (1996).
 [21] M. Kyotoku, N. Teruya, and C. L. Lima, *Phys. Lett. B* **377**, 1 (1996).
 [22] H. Sagawa, X. R. Zhou, and X. Z. Zhang, *Phys. Rev. C* **72**, 054311 (2005).
 [23] M. T. Win, K. Hagino, and T. Koike, *Phys. Rev. C* **83**, 014301 (2011).
 [24] M. T. Win and K. Hagino, *Phys. Rev. C* **78**, 054311 (2008).
 [25] E. Ha and M.-K. Cheoun, *Phys. Rev. C* **88**, 017603 (2013).
 [26] E. Ha, M.-K. Cheoun, F. Šimkovic, *Phys. Rev. C* **92**, 044315 (2015).
 [27] E. Ha and M.-K. Cheoun, *Phys. Rev. C* **94**, 054320 (2016).
 [28] E. Ha and M.-K. Cheoun, *Nucl. Phys. A* **934**, 73 (2015).
 [29] S. Cwiok *et al.*, *Computer Physics Communications* **46**, 379 (1987).
 [30] R. Noyarov, *J. Phys. G* **10**, 539 (1984).
 [31] J. Damgaard *et al.*, *Nucl. Phys. A* **135**, 432 (1969).
 [32] B. Pritychenko, M. Birch, B. Singh, and M. Horoi, *At. Data Nucl. Data Tables* **107**, 1 (2016).
 [33] B. Pritychenko, J. Choquette, M. Horoi, B. Karamy, and B. Singh, *Atom. Data Nucl. Data Tables* **98**, 798 (2012).
 [34] S. Raman, C. W. Nestor, Jr., P. Tikkanen, *At. Data and Nucl. Data Tables* **78**, 1 (2001).
 [35] G. A. Lalazissis, S. Raman, and P. Ring, *At. Data and Nucl. Data Tables* **71**, 1 (1999).
 [36] P. Moller, A. J. Sierk, T. Ichikawa, and H. Sagawa, *At. Data Nucl. Data Tables* **109-110**, 1 (2016).
 [37] N. J. Stone, *At. Data Nucl. Data Tables* **90**, 75 (2005).
 [38] T. Peach *et al.*, *Phys. Rev. C* **93**, 064325 (2016).
 [39] E. Ha and M.-K. Cheoun, *Euro. Phys. J. A* **53**, 26 (2017).
 [40] R. H. Spear, *Phys. Rep.* **73**, 369 (1981).
 [41] M. Bender, K. Rutz, P.-G. Reinhard, and J. A. Maruhn, *Euro. Phys. J. A* **8**, 59 (2000).
 [42] P. Ring, Y. K. Gambhir, and G. A. Lalazissis, *Comput. Phys. Commun.* **105**, 77 (1997).
 [43] H. Sagawa, T. Suzuki, and M. Sasano, *Phys. Rev. C* **94**, 041303(R) (2016).